Journal of Alloys and Compounds 802 (2019) 467–476

Contents lists available at ScienceDirect

Journal of Alloys and Compounds

journal homepage: http://www.elsevier.com/locate/jalcom

Composite ZIF-8 with CQDs for boosting visible-light-driven photocatalytic removal of NO

Xiaoyan Wei [a, b], Yawen Wang [a, *], Yu Huang [b, **], Caimei Fan [a]

[a] College of Chemistry and Chemical Engineering, Taiyuan University of Technology, Taiyuan, 030024, China
[b] Key Lab of Aerosol Chemistry & Physics, Institute of Earth Environment, Chinese Academy of Sciences, Xi'an, 710061, China

ARTICLE INFO

Article history:
Received 11 January 2019
Received in revised form
22 May 2019
Accepted 7 June 2019
Available online 10 June 2019

Keywords:
CQDs/ZIF-8
Photocatalysis
Visible light
NO_x
Up-conversion

ABSTRACT

Metal–organic frameworks (MOFs) with the advantage of high surface area are attracting growing concern in photocatalysis, but the limitations of no visible light response and low carrier migration efficiency also exist in MOFs materials. Carbon quantum dots (CQDs) with unique optical properties are a novel class of carbon nanomaterials, which have attracted extensive attention in the field of photocatalysis. In this work, compositing with CQDs for realizing MOFs visible-light photocatalytic NO performance was elucidated. We synthesized CQDs/ZIF-8 composite via a simple surface soaking approach, and the 0.5-CQDs/ZIF-8 composite showed the best removal performance of NO, which was ~43%. The effect of CQDs on boosting visible-light photocatalytic activity of ZIF-8 was explored based on the photocurrent test, electrochemical impedance spectra, activity tests and radical trapping experiment under different monochromatic light irradiation, up-conversion photoluminescence spectra of CQDs, and electron spin resonance spectroscopy measurement. These results demonstrated compositing with CQDs is an effective way to boost the visible-light photocatalytic activity of ZIF-8, in which CQDs improves the visible light utilization and carrier separation efficiency. Apart of that, the results fully proved that the up-conversion effect indeed played a role in driving ZIF-8 into visible light response owing to the still working holes (h^+) under 500 nm of monochromatic light irradiation. The possible NO_x removal mechanism over CQDs/ZIF-8 composite was then proposed in the work.

1. Introduction

Nitrogen oxides (NO_x) pollution to the environment has become a serious global problem, and its effect on the atmosphere mainly include the formation of acid rain, the increase of ozone concentration, and the formation of fly ash in the air [1]. In recent years, with the development of air purification technologies, environment-friendly photocatalytic oxidation technology is a promising direction for air purification under mild conditions. It is widely recognized that in a typical photocatalytic process for NO_x, the photocatalyst is excited by light with certain wavelength to generate electron-hole pairs, and then the separated electrons (e^-) and holes (h^+) transfer to the active sites to form radicals to react with NO_x that adsorbed on the surface of catalysts [2].

The activity of catalysts is closely related to its surface area [3,4]. With the development of traditional semiconductor photocatalysts [5], a class of newly-developed inorganic-organic hybrid porous materials, namely metal–organic frameworks (MOFs) have been rapidly developed. There are many excellent properties of MOFs, such as high surface area and excellent adsorptive performance, well-defined crystalline structures and much wider chemical and structural modularity [6,7]. Therefore, MOFs-based materials are always applied in the fields of gas adsorption, catalysis, drug delivery, sensing [8,9] and so on [10]. Zeolite Imidazole Frameworks (ZIFs) are made up of metal ions (such as Zn^{2+}, Co^{2+}) with imidazole or imidazole ligand [11]. Especially ZIF-8, which has a broad application prospect particularly due to the advantages of large surface area, thermal and chemical stability and facile synthetic method [12,13], and is generally used as cocatalyst or host matrices by simply utilizing the adsorption capability of ZIF-8 shells [14,15]. In recent years, the application of MOFs materials has expanded into photocatalytic dye degradation [16], CO_2 reduction [17] and hydrogen production [18]. Recent years, Wang et al. firstly described the performance of pristine ZIF-8 for photocatalytic

* Corresponding author.
** Corresponding author.
E-mail addresses: wangyawen@tyut.edu.cn (Y. Wang), huangyu@ieecas.cn (Y. Huang).

https://doi.org/10.1016/j.jallcom.2019.06.086
0925-8388/

degradation of methylene blue (MB) under UV illumination, and the photocatalytic mechanism can be illustrated by HOMO-LUMO theory [19]. However, the application of MOFs in visible-light driven photocatalysis has been hindered due to the large band gap energy and low photo-induced carrier mobility [20–25]. In order to make ZIFs act directly as a visible-light responsive photocatalyst, Zhang et al. developed copper doped ZIF-67 material and studied the visible light driven photocatalytic degradation of MO in the presence of H_2O_2 [26]. Recently, Co doping in tuning the optical property and visible light photocatalytic activity of ZIF-8 for dye degradation was also demonstrated by Mohamad et al. [27]. However, despite doping metal ions can broaden the light absorption effectively, it is hard to increase the separating efficiency of photoexcited carriers at the same time [28]. In addition, doping metal ions has possible to increase the risk of introducing new sources of pollution to environment. Therefore, more work needs to be done in the development of green visible light responsive MOFs-based materials.

Carbon quantum dot (CQDs) is a new type of fluorescent carbon nanomaterial, which displays many excellent properties, such as non-toxic, ultraviolet–visible absorption, photoluminescence properties, photo-induced electron transfer and unique up-conversion photoluminescence (UCPL) properties, and has been widely used in the field of photocatalysis [29–31]. Compositing with CQDs has been proved to be an effective and green way to improve the carrier separation efficiency and drive photocatalysts into visible light response due to the photosensitization [32] or up-conversion effect of CQDs [33].

Therefore, under the premise of maintaining structural stability and large specific surface area of ZIF-8, for providing it with a new possibility of visible light response, we proposed to incorporate CQDs with ZIF-8 by surface soaking modification method. The photocatalytic activity of CQDs/ZIF-8 composites under visible light was tested by removing gaseous NO in continuous air flow. The reason for the visible light response of ZIF-8 was deeply studied and the results demonstrated the CQDs can improve the carrier separation efficiency and the up-conversion effect of it did play a role in driving ZIF-8 into visible light response.

2. Experimental section

2.1. Materials

All reagents were of analytical grade, purchased from Aladdin (Shanghai, China) and used without further purification.

2.2. Synthesis of CQDs/ZIF-8 composites

CQDs/ZIF-8 composites were synthesized by using a simple surface soaking method. That is, 0.2 g ZIF-8 was immersed into 20 mL methanol and the solution was ultrasonic assisted diffusion for 10 min, then CQDs solution was added and magnetic stirring for 30 min. Finally, the products were washed with methanol for 3 times, and then dried at 60 °C. CQDs/ZIF-8 composites with CQDs content of 0.1 mL (0.5 vol%), 0.5 mL (2.5 vol%) and 2.0 mL (10 vol%) were synthesized and denoted as 0.1-CQD/ZIF-8, 0.5-CQD/ZIF-8 and 2.0-CQD/ZIF-8, respectively.

CQDs was synthesized through an hydrothermal method [34], as described in supporting information. The synthesis of ZIF-8 was similar to the typical method [35], in brief, 0.561 g of zinc hydroxide ($Zn(OH)_2$) and 1.854 g of 2-methylimidazole (HmIm) were dissolved in 100 mL ammonium hydroxide ($NH_3 \cdot H_2O$) and 40 mL methanol, respectively. Then the solution of HmIm in methanol was slowly and carefully layered onto a solution of $Zn(OH)_2$ in ammonium hydroxide ($NH_3 \cdot H_2O$). After two days, the resulted solid product was collected via centrifugation and washed with methanol/H_2O (1:1 V/V) for several times, then dried at 60 °C.

2.3. Characterizations

The powder X-ray diffraction (XRD) patterns were performed using a Philips X'pert PRO SUPER diffractometer with Cu Kα ($\lambda = 1.54178$ Å) radiation. The morphologies of resulting samples were characterized by a field emission scanning electron microscopy (SEM) (JEOL JSM-6490, Japan) and transmission electron microscopy (TEM) (JES-3010, Japan). Chemical composition of the samples was analyzed using X-ray photoelectron spectroscopy (XPS, Thermo Escalab 250Xi, USA). The binding energies were normalized to the signal for adventitious carbon at 284.8 eV. The Brunauer-Emmett-Teller (BET) surface area and pore structure of resulted samples were obtained from N_2 adsorption/desorption isotherms at 77 K (ASAP 2020 automatic analyzer). The samples were degassed at 110 °C prior to analysis. UV–Vis Diffused Reflectance Spectrum (UV–Vis DRS) of the resulted samples were performed on a Varian Cary 100 Scan UV–Visible system equipped with a labsphere diffuse reflectance accessory in the wavelength range of 200–800 nm, and using Ba_2SO_4 reflection as a reference. The up-conversion photoluminescence (UCPL) spectra of CQDs was recorded on a Horiba Fluoromax-4 (France) luminescence spectrometer using a Xe lamp as the excitation source. Samples for electron spin resonance spectroscopy (ESR, ER200-SRC, Bruker, Germany) were prepared by dispersing 0.05 g of photocatalyst into 25 mM 5, 5′-dimethyl-1-pirroline-N-oxide (DMPO) solution for DMPO- $^{\bullet}OH$ or 50 mL methanol dispersion for DMPO- $^{\bullet}O_2^-$, respectively. The light irradiation source was a 300 W Xe arc lamp (PLS-SXE 300, Beijing). The visible light used in this study was obtained by cutting UV light ($\lambda < 420$ nm) with an optical filter.

2.4. Photoelectrochemical measurements

Photoelectrochemical properties of the as-prepared samples were evaluated using a Parstat 4000 electrochemical workstation (USA) in a conventional three-electrode cell, with a platinum plate as the counter electrode and an Ag/AgCl electrode as the reference electrode. The working electrode was prepared by dispersing the 20 mg sample into 4 mL Nafion ethanol solution to obtain homogeneous suspension by using the ultrasonic dispersion method for 30 min. The suspension was coated onto a F-doped tin oxide-conducting glass and dried at room temperature. The photocurrent-time curves were measured at 0.2 V versus Ag/AgCl electrode in 0.5 mol/L Na_2SO_3 at ambient temperature under a 300 W Xe lamp ($\lambda = 420$ nm). Electrochemical impedance spectroscopy (EIS) of the samples were measured at a frequency range of 0.1 Hz–100 kHz with an 5 mV voltage amplitude under an open-circuit voltage in a 1.0 mmol/L $K_3Fe(CN)_6$ and $K_4Fe(CN)_6$ solution.

2.5. Evaluation of photocatalytic activity

The photocatalytic NO oxidation of the as-prepared samples was performed at ambient temperature in a continuous flow reactor equipped with an online NO–NO_2–NO_x analyzer (Model 42c, Thermo Environmental Instruments Inc., Franklin, MA, USA). The reactor has a volume capacity of 4.5 L (30 cm × 15 cm × 10 cm). A 300 W commercial Xe arc lamp equipped with a UV cut filter to cut off lights with wavelength <420 nm or monochromatic light filter (microsolar 300, Perfectlight, China) was vertically placed outside the reactor. Gaseous No was supplied by a compressed gas cylinder at a concentration of 48 ppm (N_2 balance) in accordance with the standard of the National Institute of Standards and Technology. The initial NO concentration was diluted to 420 ppb by an air stream

supplied by a zero-air generator (Model 1001, Sabio Instruments LLC, Georgetown, TX, USA), and the flow rate was controlled at 2 L/min. The concentrations of NO and NO_2 were continuously monitored using the NO analyzer at a sampling rate of 0.6 L/min. The desired relative humidity level of NO flow was controlled by passing zero air streams through a humidification chamber.

For photocatalytic test, 0.1 g of photocatalyst (ZIF-8, CQDs, P25, CQDs/ZIF-8 composites) was dispersed in 10 mL water to form a homogeneous suspension, then coated onto one dish (10.0 cm in diameter), which was subsequently pretreated at 60 °C to steam up the water and cooled to room temperature before the photocatalytic test. The adsorption-desorption equilibrium was achieved before the lamp was turned on. The removal ratio (η) of NO was calculated as $\eta\ (\%) = (1-C/C_0) \times 100\%$, where C_0 represents the initial concentration of NO, that is, the concentration at adsorption equilibrium, and C represents the concentration at a certain time in the photocatalytic reaction.

3. Results and discussion

3.1. Phase structure, surface elemental composition and morphology

The prepared ZIF-8 and CQDs/ZIF-8 composites with different CQDs contents were characterized via XRD. As shown in Fig. 1, the synthesized ZIF-8 is consistent with the simulated ZIF-8 pattern [36], the strong peaks at 2θ values of 7.3°, 10.3°, 12.7°, 14.7°, 16.4 18.0°, 24.6° and 26.7° are ascribed to the (011), (002), (112), (022), (013), (222), (233) and (134) reflections of ZIF-8, respectively [37]. The phase purity was not affected by the introduction of CQDs, and the XRD of composites do not show the characteristic peak for CQDs (at 26°), which may due to the high dispersion and low content of the CQDs in the composites, and similar situation also exists in other jobs [38].

In order to check the chemical states of the elements in the prepared samples, we carried out XPS of the samples. As seen in Fig. 2a, the XPS pattern of ZIF-8 confirms the presence of Zn, N and C elements. Fig. 2b shows the Zn 2*p* spectra exhibit two intense peaks at 1022.8 eV and 1046.1 eV, which corresponding to the $2p_{3/2}$ and $2p_{1/2}$ components [39,40], respectively. However, after the loading of CQDs, the location of the peaks for Zn 2*p* accompany by a slight shift of 0.3 eV to lower binding energy, reflecting Zn become less oxidized due to the decoration of CQDs, and resulting in an increased electron density on Zn [41], which implies that the Zn may be involved in the interaction of two components. The C 1*s* spectra in Fig. 2c is divided into two peaks at 284.8 eV and 285.8 eV, which can be assigned to the C-C bond with sp^2 orbital and C-N bond [42], respectively. The symmetric peak at 398.9 eV in N 1*s* spectra (Fig. 2d) of ZIF-8 is assigned to 2-methylimidazole [43].

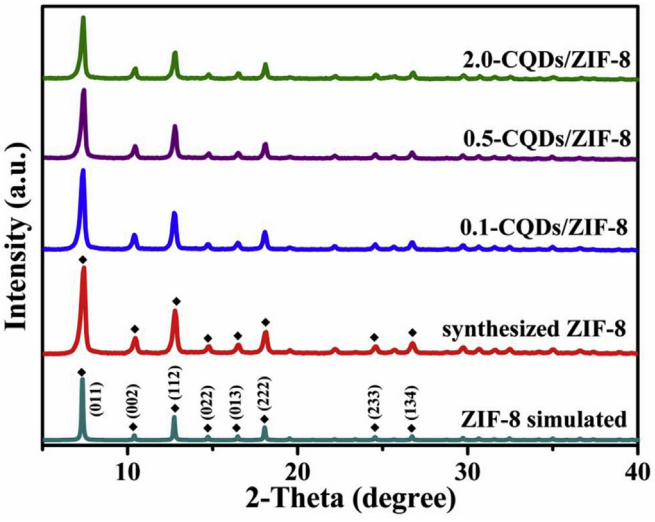

Fig. 1. XRD patterns of pure ZIF-8 and CQDs/ZIF-8 composites with different CQDs contents.

We further measured the TEM images of the as-synthesized materials and the HR-TEM image of the composite, as shown in Fig. 3. In Fig. 3a, the as-prepared ZIF-8 sample with a size approximately 20–150 nm and an irregular edge outline (inset in Fig. 3a). Fig. 3b shows that CQDs nanoparticles are 2–10 nm in size, and we can see from the TEM image that they are all monodispersed spherical nanoparticles. Furthermore, we calculate the size of 300 nanoparticles and obtained the particle size distribution map, as can be seen from the inset of Fig. 3b, the size is mainly distributed around 4–6 nm. Fig. 3c shows the TEM image of 0.5-CQDs/ZIF-8 composite, the particle size is not uniform and there is no obvious change in morphology after the loading of CQDs, this is also in consistent with SEM image in Fig. S1. To determine if CQDs is incorporated into the composite, Fig. 3d shows the HR-TEM image of the composite, which is the area marked in Fig. 3c, the particle at the edge of ZIF-8 particles shows the lattice spacing of 0.32 nm, corresponding to the (002) plane of graphite carbon. This result also confirms the successful loading of CQDs into ZIF-8.

3.2. Porous structure and optical properties

In general, photocatalytic reaction occurs on the outer surface of catalysts, the activity of catalysts closely related to the surface area, the larger the specific surface area of the catalyst, the more active adsorption centers it can use [44]. N_2 adsorption/desorption isotherms of ZIF-8 and 0.5-CQDs/ZIF-8 composite were shown in Fig. 4. It is found the isotherm of ZIF-8 and 0.5-CQDs/ZIF-8 all with a steep increase at low pressure (P/P_0), suggesting they are a typical type-I behavior and there is a microporous structure [45]. ZIF-8 and 0.5-CQDs/ZIF-8 composite with BET surface areas of 1355.59 m^2/g and 1479.05 m^2/g, the BET surface area of increased about 123.5 m^2/g, the increased surface area indicating that the composite may provide more active sites for photocatalytic reaction [46]. The results of BET surface area, pore volume and pore size distribution were shown in Table 1, these results indicating that ZIF-8 maintain its big surface area and the stability of pore structure after the incorporation of CQDs.

The UV–Vis DRS was performed to investigate the optical property of the prepared samples, as shown in Fig. 5a, ZIF-8 exhibits a strong UV light absorption at approximately 200 nm, indicating that ZIF-8 may has an excellent UV photocatalytic performance, and the absorption edge is approximately at 400 nm. CQDs typically show obvious optical absorption property [34], the UV–Vis absorption result of CQDs solution showed that there is an obvious optical absorption from ultraviolet to visible region. After the incorporation of CQDs, the composite have a stronger absorption compared with pristine ZIF-8, and the visible light absorption significantly improved, indicating that CQDs with strong light absorption property contributed to the enhanced light absorption. The enhanced light absorption also reflects the loading of CQDs into ZIF-8. According to the Kubelka–Munk equation $Ah\nu = k(h\nu\text{-}Eg)^{1/2}$, the band-gap energy ($E_g$) of ZIF-8 is estimated to be 3.1 eV via the insert $(Ah\nu)^2$ vs $h\nu$ curve of ZIF-8 in Fig. 5b [47,48]. As shown in Fig. 5b, the XPS valence band spectra determines that the valence band (VB) edge of ZIF-8 is located at about 2.0 eV, which is more negative than E_0 ($OH^-/{}^{\bullet}OH$) (2.38 eV vs. NHE), as described in the previous study [49].

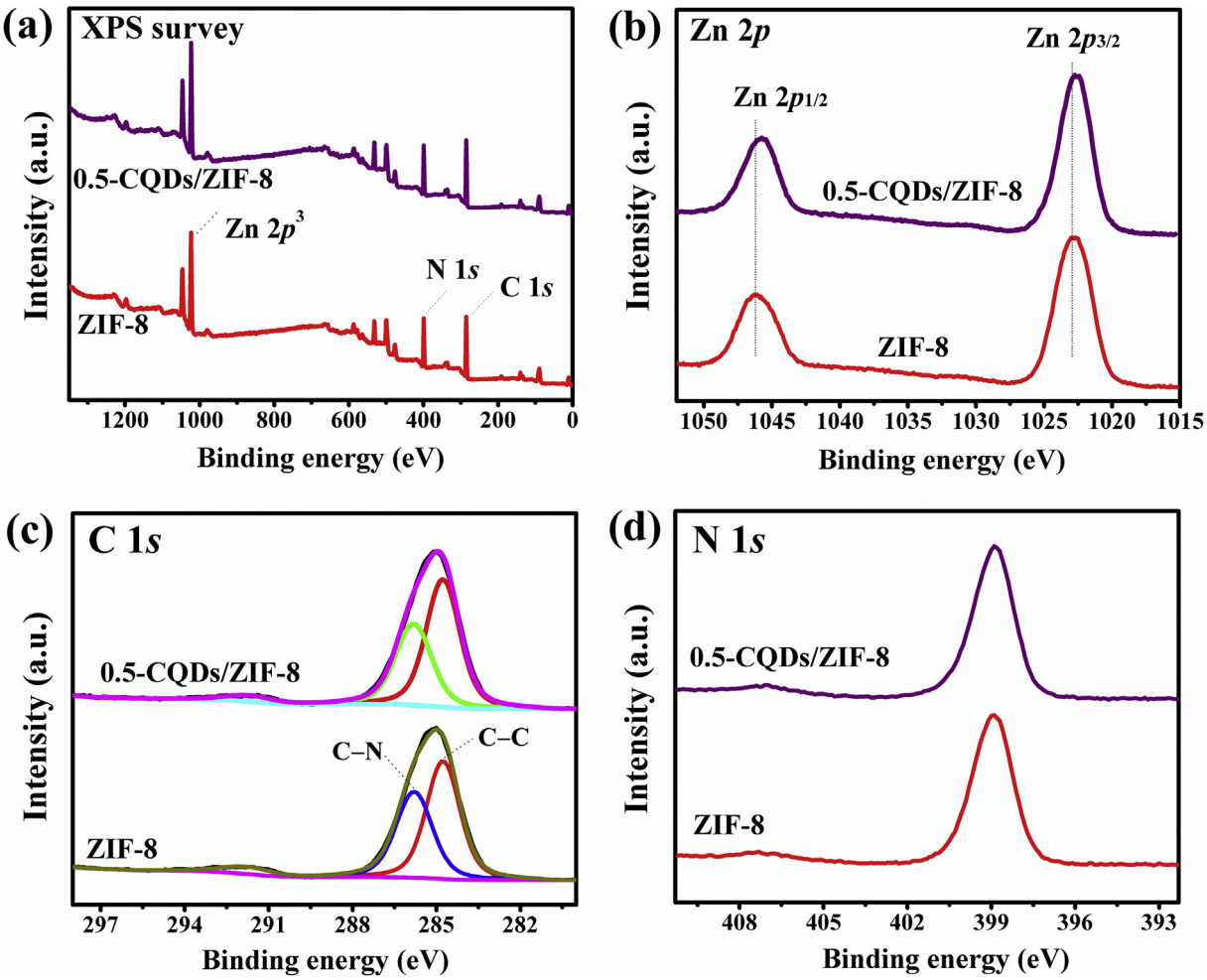

Fig. 2. (a) XPS survey spectra of ZIF-8 and 0.5-CQDs/ZIF-8. (b) Zn 2*p* spectra. (c) C 1*s* spectra and (d) N 1*s* spectra.

3.3. Evaluation of photocatalytic activity

We evaluated the photocatalytic NO degradation efficiency under visible light irradiation with online NO_x analyzer, 0.1 g photocatalyst was used in the photocatalytic reaction and the lamp equipped with a 420 nm filter was turned on after the adsorption-desorption equilibrium was achieved. As observed from the activity tests (Fig. 6a), no nitric oxide can be converted in the absence of photocatalyst. For ZIF-8, it exhibits almost no NO removal performance under visible light irradiation due to the wide band gap of ZIF-8, and it is also inactive for single CQDs under visible light irradiation. While CQDs/ZIF-8 composites with different loading amount of CQDs all exhibit enhanced NO removal efficiency than pristine ZIF-8. The removal efficiency is improved with the increase of CQDs loading amount, and the best performance is achieved for 0.5-CQDs/ZIF-8, about 43% of initial nitrogen oxide is removed with relatively lower NO_2 yield compared with commercial P25 as shown in Fig. 6b. However, excessive loading is not conducive to the enhancement of photocatalytic performance. When the CQDs loading amount is further increased to 2 mL, the photocatalytic activity is decreased. In any case, the introduction of CQDs can significantly drive ZIF-8 into visible-light-responding. Furthermore, the effect of catalyst dosage on the photocatalytic activity was also conducted, as shown in Fig. 6c, the photocatalytic efficiency increased with the increase of the amount of catalyst until exceeded 0.3 g. The activity of 0.3 g sample was the same as that of 0.2 g, probably due to the lighting area is limited by the diameter of dish used in photocatalytic activity test, the sample is too thick in the dish to make full use of the sunlight. Fig. 6d shows the photocatalytic stability of 0.5-CQDs/ZIF-8 sample for photocatalytic removal of NO, as seen there is a 9% reduction in activity after 3 cycles. Considering that the decrease in activity may be caused by the NO_3^- occupy the active sites on catalyst, we refreshed the 0.5-CQDs/ZIF-8 by washing with deionized water. As expected, the activity recovered a lot (fourth run in Fig. 6d). In other words, the photoactivity performance of 0.5-CQDs/ZIF-8 could regenerated by water.

3.4. Effect of CQDs

According to the experimental results, we believe that CQDs play a crucial role for the enhanced photocatalytic activity under visible light irradiation.

The transient photocurrent response of ZIF-8 and 0.5-CQDs/ZIF-8 under intermittent visible-light irradiation are conducted to determine the separation efficiency of carriers. As shown in Fig. 7a, ZIF-8 exhibits a weak transient photocurrent response, whereas 0.5-CQDs/ZIF-8 shows much stronger transient photocurrent response, which is approximately 1.6 times stronger. The relative size of the radius of the arc in EIS corresponds to the size of the charge transfer resistance and the separation efficiency of the photogenerated electron-hole pairs [50]. As seen in EIS, the 0.5-

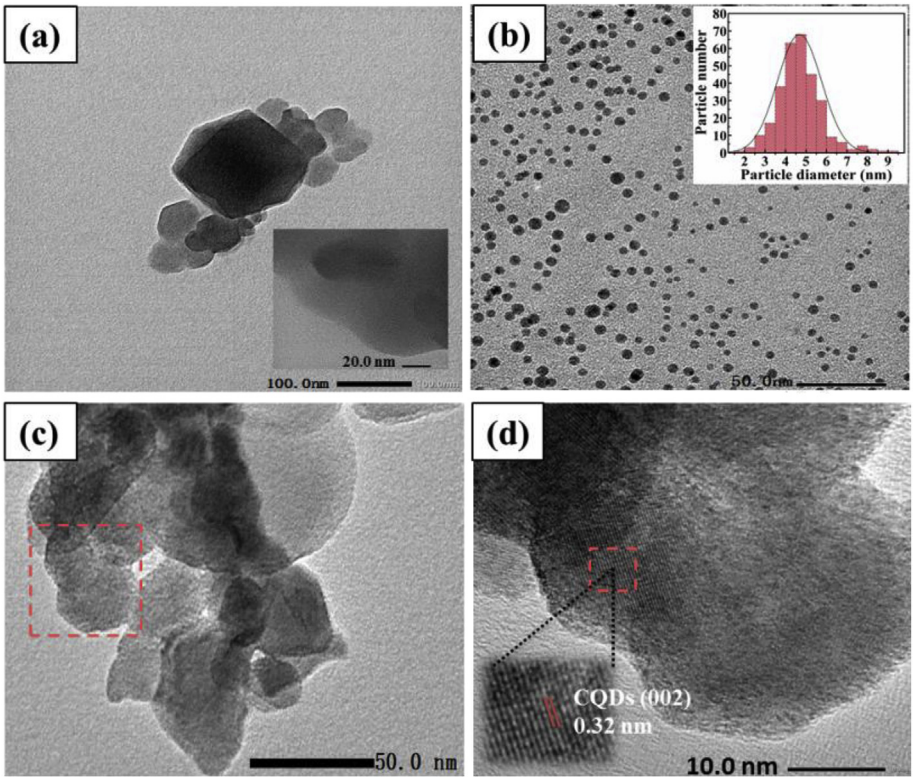

Fig. 3. (a) TEM image of ZIF-8 (the insert image is the edge image of ZIF-8 sample). (b) TEM image of pure CQDs (the inset is the size distribution map of 300 nanoparticles in this image). (c) TEM image of 0.5-CQDs/ZIF-8 composite. (d) HR-TEM image of the composite labeled area in (c). (the enlarged area is the lattice fringe of CQDs).

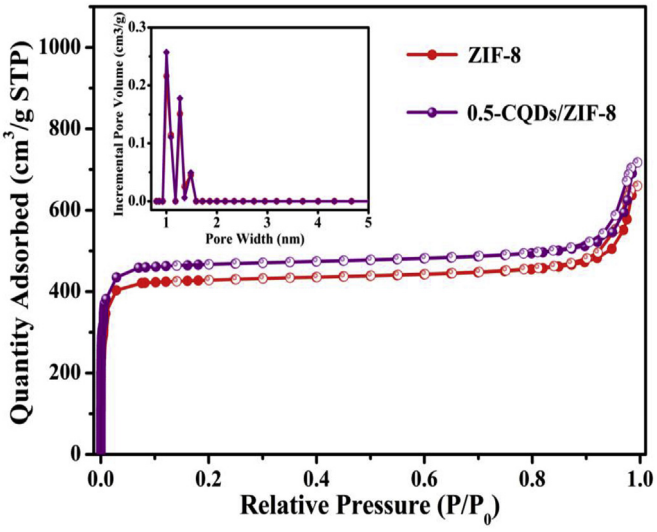

Fig. 4. N_2 adsorption/desorption curves of ZIF-8 and 0.5-CQDs/ZIF-8 (The inset shows the curves of Incremental Pore Volume vs. Pore Width).

CQDs/ZIF-8 composite has a smaller radius than ZIF-8. On another note, the result of EIS in Fig. 7b indicating that the charge transfer resistance and separation efficiency of electron-hole pairs in 0.5-CQDs/ZIF-8 are improved. There could be two possible reasons for the result. One reason is the separate efficiency of electron-hole pairs is improved [51], another reason is the numbers of photo-generated charge carriers are increased.

In order to further detect which reason or both of them caused stronger transient photocurrent response of 0.5-CQDs/ZIF-8, we measured the photocatalytic activity of ZIF-8 and 0.5-CQDs/ZIF-8 under different monochromatic light irradiation (Fig. 7c). Under 365 nm UV light irradiation, ZIF-8 shows a NO removal efficiency of 7.1%, while 0.5-CQDs/ZIF-8 has an activity of 18.3%. Obviously, under 365 nm UV light irradiation, the up-conversion or photosensitization effect of CQDs will not work. Therefore this result also proves CQDs, as electron mediators, can promote the separation efficiency of electron-hole pairs of photocatalysts as other researcher reported [52]. In Fig. 7c, a very interesting result is found, ZIF-8 shows almost no activity under all visible monochromatic light irradiation, however, 0.5-CQDs/ZIF-8 composite exhibits effective NO removal efficiency of 16.8, 9.7 and 4.2% under 500, 550 and 600 nm of monochromatic light irradiation,

Table 1
Comparison of BET surface area, pore volume and pore size distribution for ZIF-8 and 0.5-CQDs/ZIF-8 composite.

Material	BET surface area (m^2/g)	Pore volume (cm^3/g)	Pore size (nm)
ZIF-8	1355.59	0.611	1.940
0.5-CQDs/ZIF-8	1479.05	0.670	1.942

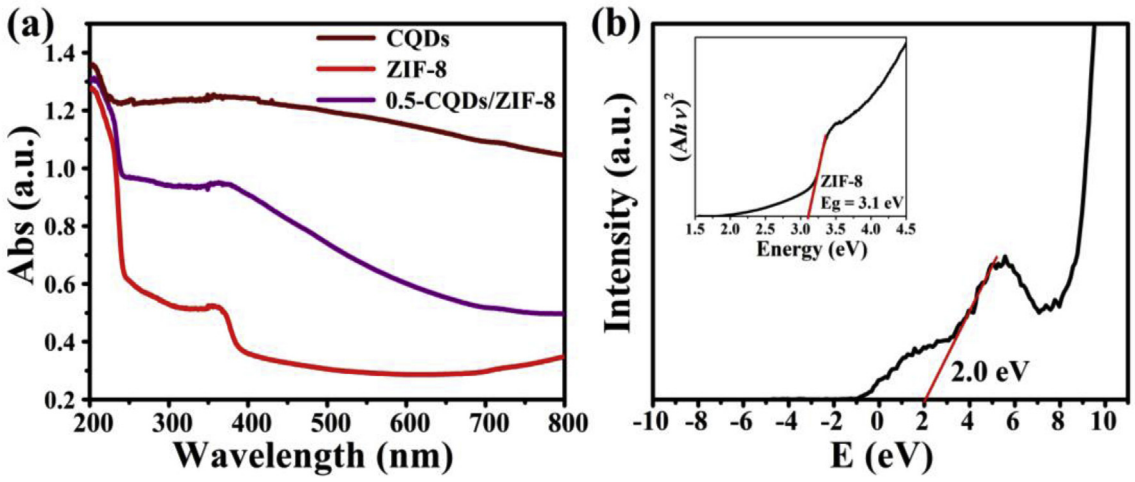

Fig. 5. (a) UV–Vis absorption or DRS of CQDs, pristine ZIF-8 and 0.5-CQDs/ZIF-8 composite. (b) XPS valence band spectra of ZIF-8. Insert in (b) is $(Ah\nu)^2$ vs $h\nu$ curve of ZIF-8.

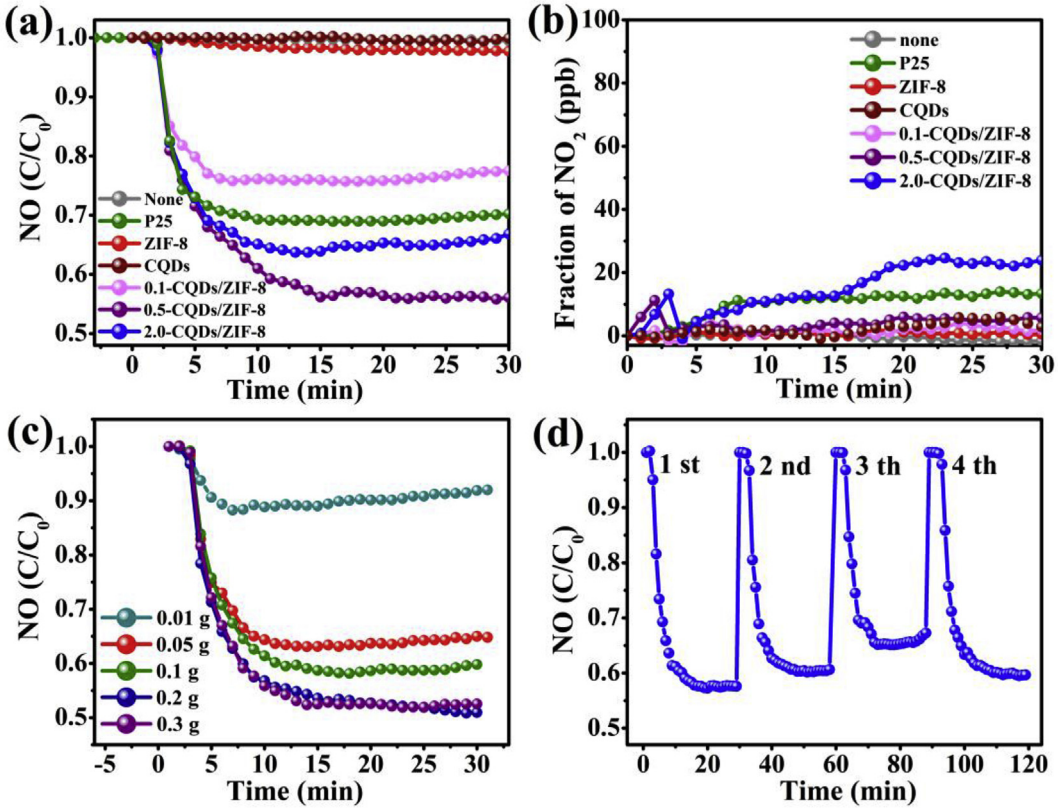

Fig. 6. (a) Photocatalytic NO degradation efficiency of ZIF-8, P25, CQDs and CQDs/ZIF-8 composites under visible light irradiation ($\lambda \geq 420$ nm). (b) The corresponding NO_2 yield. (c) The effect of different amount of 0.5-CQDs/ZIF-8 photocatalyst on the removal efficiency of NO under visible light irradiation. (d) The cyclic stability of 0.5-CQDs/ZIF-8 photocatalyst for removing NO under visible light irradiation.

respectively. Even at 700 nm light irradiation, there is still a removal efficiency of 2.0%. Therefore, the introduction of CQDs not only can promote the separation efficiency of electron-hole pairs but also can increase the excited electron-hole pairs under visible light irradiation, which thereby result in stronger transient photocurrent response.

It has been reported that both up-conversion [46] and photo-sensitization effect [53,54] of CQDs can result in the visible-light responsive photocatalytic activity of photocatalysts. In this work, we try our best to detect the role of CQDs that might be played in driving ZIF-8 as a visible-light responsive photocatalyst.

Firstly, we characterized the UCPL spectra of CQDs, as shown in Fig. 7d, it can be seen that a short wave-length light of 350–600 nm can be emitted when CQDs was excited by light having a wavelength of 500–900 nm, and the emitted light covers part of ultraviolet area. This result indicates that the prepared CQDs have up-conversion effect, which may play a role in driving ZIF-8 into visible light response. Then we test the possible active radicals by using different

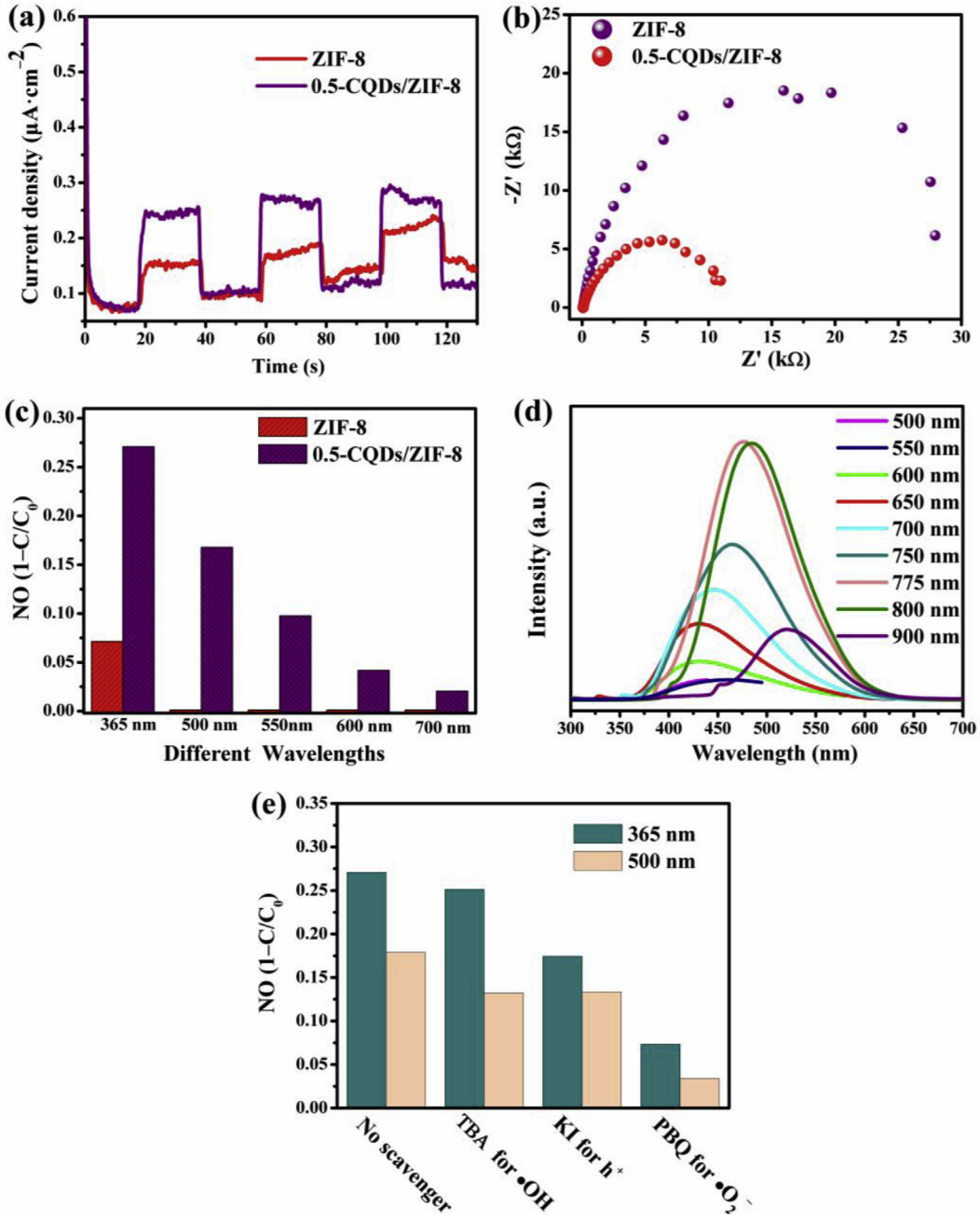

Fig. 7. (a) Transient photocurrent responses of ZIF-8 and 0.5-CQDs/ZIF-8 under visible light irradiation. (b) EIS of ZIF-8 and 0.5-CQDs/ZIF-8. (c) NO removal efficiency of ZIF-8 and 0.5-CQDs/ZIF-8 under monochromatic light irradiation at wavelengths of 365 nm, 500 nm, 550 nm, 600 nm, and 700 nm for 30 min, respectively. (d) UCPL spectra of prepared CQDs. (e) Radical-trapping experiments under 365 and 500 nm of monochromatic light irradiation.

radical scavengers under 365 and 500 nm of monochromatic light irradiation, separately, as seen from Fig. 7e. The addition of p-benzoquinone (PBQ) has strong inhibitory effect (about 73% under 365 nm ultraviolet light irradiation and 77% under 500 nm visible light irradiation) on the photocatalytic activity. The inhibition efficiency of potassium iodide (KI) on photocatalytic performance is 29% and 20% under 365 nm ultraviolet light and 500 nm visible light irradiation, and for addition of tert butyl alcohol (TBA) is 9% and 19%, respectively. The results indicate the active radical species are similar under 365 nm ultraviolet light and 500 nm visible light irradiation, where despite $^{\bullet}O_2^-$ is the main active radical, h^+ and $^{\bullet}OH$ also play a role in removing NO. According to $E_{VB} - E_{CB} = E_g$, the conduction band (CB) of ZIF-8 is calculated to be at − 1.1 eV (vs. NHE), which is more negative than E_0 ($O_2/^{\bullet}O_2^-$) (−0.33 eV vs. NHE), so the $^{\bullet}O_2^-$ should be formed by reacting photogenerated e^- with surface oxygen (Eq. (3)). The VB edge of ZIF-8 is located at approximately 2.0 eV, which is not more positive than E_0 ($OH^-/^{\bullet}OH$) (2.38 eV vs. NHE), therefore $^{\bullet}OH$ may attributed to the reduction of $^{\bullet}O_2^-$ [55]. The DMPO spin-trapping ESR spectra of 0.5-CQDs/ZIF-8 in Fig. 8 also shows the existence of $^{\bullet}O_2$ and $^{\bullet}OH$, and the enhancing signals with the extension of irradiation time. If the visible-light-driven property of ZIF-8 is caused totally by photosensitization effect of CQDs, the h^+ should not work at all under visible light irradiation. For example, Zhang et al. found that CQDs mainly donate e^- to the conduction band of the photocatalyst under long wavelength irradiation ($\lambda > 450$ nm), enabling wide band gap photocatalyst to

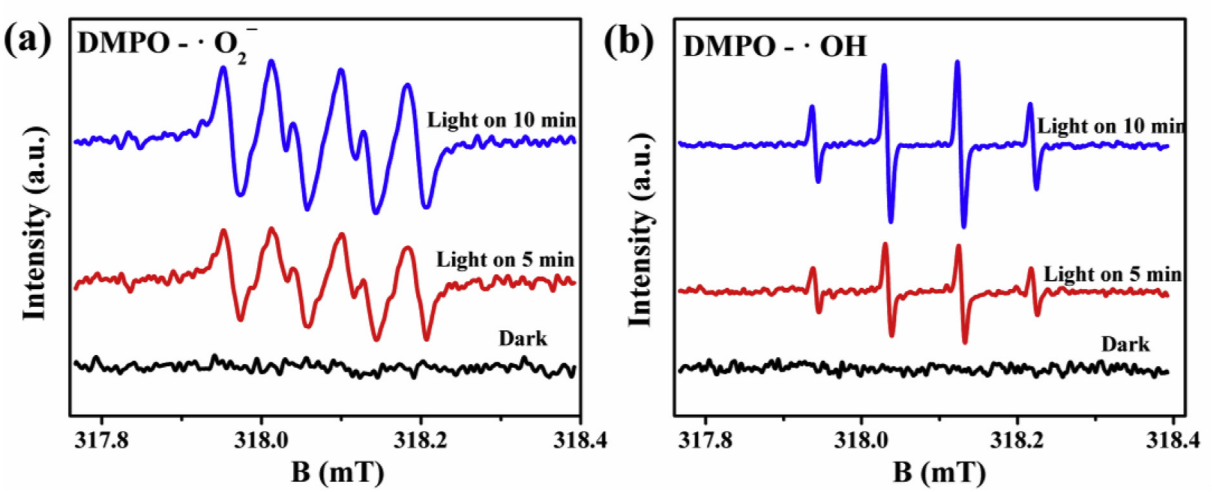

Fig. 8. DMPO spin-trapping ESR spectra of as-synthesized 0.5-CQDs/ZIF-8 in the dark and under visible light irradiation for (a) $^{\bullet}O_2^-$ and (b) $^{\bullet}OH$.

be visible-light responsive. That means h^+ do not involve in the photocatalytic reaction when CQDs serves as a photosensitizer [32]. Therefore, in this study, we cannot completely rule out the photosensitization effect of CQDs due to the main active radical of ZIF-8 is happened to be $^{\bullet}O_2^-$ under UV light irradiation, but can be sure that the up-conversion effect indeed play a role in driving ZIF-8 into visible light response owing to the still working h^+ under 500 nm of monochromatic light irradiation.

3.5. The possible photocatalytic oxidation pathway

For MOFs, the photocatalytic process is occurring between the highest occupied molecular orbital (HOMO) and the lowest unoccupied molecular orbital (LUMO) [56–58]. The organic linkers (HOMO) can act as VB and the metal clusters (LUMO) corresponding to CB, respectively. MOF-5 is the first example to be used as an efficient photocatalyst, with e^- in the CB and h^+ in the VB [59]. Similar to MOF-5, the structure of ZIF-8 contains tetrahedra of Zn_4N, the HOMO is mainly owing to the N 2*p* bonding orbitals (VB), which form the imidizole linker, and the LUMO is mainly contributed by empty Zn orbitals (CB) [19,60]. Then, based on these results, a possible NO oxidation pathway and schematic model over CQDs/ZIF-8 are proposed as follows: CQDs absorb long wavelength light and emit short wavelength light, thus, ZIF-8 can efficiently harvest the visible light from the up-conversion effect of CQDs to form photogenerated electron-hole pairs (Eq. (1)) [61]. Then e^- jump from the VB to the CB of ZIF-8 [62], which can combine with O_2 adsorbed on the surfaces of photocatalyst to form $^{\bullet}O_2^-$ (Eq. (3)), and some of $^{\bullet}O_2^-$ may transform to $^{\bullet}OH$ (Eq. (4) and (5)) [30,52,63]. Then h^+, $^{\bullet}O_2^-$ and $^{\bullet}OH$ can react with NO in synergy to form NO_2 and further be oxidized to NO_3^- (Eqs. (2) and (5)–(7)).

The possible NO photocatalytic oxidation pathway on the surface of 0.5-CQDs/ZIF-8 photocatalyst under visible light irradiation:

CQDs (up-conversion): $\lambda_{\text{Visible light}} \rightarrow \lambda_{\text{UV-Vis light}}$

$$\text{ZIF-8} + h\nu \rightarrow e^- + h^+ \quad (1)$$

$$h^+ + NO \rightarrow NO_3^- \quad (2)$$

$$e^- + O_2 \rightarrow {}^{\bullet}O_2^- \quad (3)$$

$$^{\bullet}O_2^- + 2H^+ + 2e^- \rightarrow H_2O_2 \quad (4)$$

$$H_2O_2 + e^- \rightarrow {}^{\bullet}OH + OH^- \quad (5)$$

$$^{\bullet}O_2^- + NO_x \rightarrow NO_3^- \quad (6)$$

$$2\ {}^{\bullet}OH + NO \rightarrow NO_2 + H_2O \quad (7)$$

$$NO_2 + {}^{\bullet}OH \rightarrow NO_3^- + H^+ \quad (8)$$

Schematic model

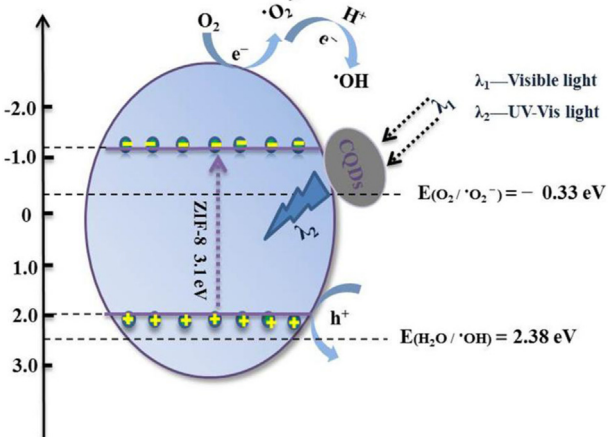

4. Conclusions

In this work, ZIF-8 was used as a main photocatalyst for NO oxidation, in view of it is only active under UV illumination due to the wide optical band gap, we used CQDs to modify ZIF-8, and the prepared CQDs/ZIF-8 composites displayed an obviously enhanced photocatalytic activity under visible light irradiation. The CQDs/ZIF-8 composite showed stronger photocurrent response than pristine ZIF-8, because CQDs in CQDs/ZIF-8 photocatalytic system can serve as electron mediators to promote the separation efficiency and increase the excited electron-hole pairs under visible light irradiation, which was confirmed by the activity test under different monochromatic light irradiation. In addition, the effect of CQDs on driving ZIF-8 into visible light response and enhancing the charge

separation efficiency was deeply studied through radical trapping experiment under 365 nm and 500 nm of monochromatic light irradiation. The results fully proved that the up-conversion effect indeed played a role in driving ZIF-8 into visible light response owing to the still working holes under 500 nm of monochromatic light irradiation. This study indicates that compositing with CQDs would be a good choice to design and synthesize green visible light responsive MOFs-based photocatalysts, and provides a possible way to see if the up-conversion effect of CQDs really plays a role in driving photocatalysts into visible light response.

Acknowledgements

This research was financially supported by the National Natural Science Foundation of China (grant number 21303116, 21676178, 21706179) and Outstanding young academic leaders of Shanxi Provincial Department of Education (grant number 154010141-s). Yu Huang was also supported by the "Hundred Talent Program" of the Chinese Academy of Sciences.

Appendix A. Supplementary data

Supplementary data to this article can be found online at https://doi.org/10.1016/j.jallcom.2019.06.086.

References

[1] W. Zhang, Q. Zhang, F. Dong, Visible-light photocatalytic removal of NO in air over BiOX (X = Cl, Br, I) single-crystal nanoplates prepared at room temperature, Ind. Eng. Chem. Res. 52 (2013) 6740–6746.
[2] H. Huang, X. Li, J. Wang, F. Dong, P.K. Chu, T. Zhang, Y. Zhang, Anionic group self-doping as a promising strategy: band-gap engineering and multi-functional applications of high-performance CO_3^{2-}-doped $Bi_2O_2CO_3$, ACS Catal. 5 (2015) 4094–4103.
[3] D. Chen, H. Xing, C. Wang, Z. Su, Highly efficient visible-light-driven CO_2 reduction to formate by a new anthracene-based zirconium MOF via dual catalytic routes, J. Mater. Chem. 4 (2016) 2657–2662.
[4] J. Zhao, C. Chen, W. Ma, Photocatalytic degradation of organic pollutants under visible light irradiation, Top. Catal. 35 (2005) 269–278.
[5] Q. Xu, J. Feng, L. Li, Q. Xiao, J. Wang, Hollow $ZnFe_2O_4/TiO_2$ composites: high-performance and recyclable visible-light photocatalyst, J. Alloy. Comp. 641 (2015) 110–118.
[6] Y. Liu, Z. Tang, Multifunctional nanoparticle@MOF core-shell nanostructures, Adv. Mater. 25 (2013) 5819–5825.
[7] J.L.C. Rowsell, O.M. Yaghi, Metal–organic frameworks: a new class of porous materials, Microporous Mesoporous Mater. 73 (2004) 3–14.
[8] W. Gao, Y. Jing, J. Yang, Z. Zhou, D. Yang, J. Sun, J. Lin, R. Cong, T. Yang, Open-framework gallium borate with boric and metaboric acid molecules inside structural channels showing photocatalysis to water splitting, Inorg. Chem. 53 (2014) 2364–2366.
[9] L. He, T. Wang, J. An, X. Li, L. Zhang, L. Li, G. Li, X. Wu, Z. Su, C. Wang, Carbon nanodots@zeolitic imidazolate framework-8 nanoparticles for simultaneous pH-responsive drug delivery and fluorescence imaging, CrystEngComm 16 (2014) 3259.
[10] W. Bao, Z. Zhang, Y. Qu, C. Zhou, X. Wang, J. Li, Confine sulfur in mesoporous metal–organic framework @ reduced graphene oxide for lithium sulfur battery, J. Alloy. Comp. 582 (2014) 334–340.
[11] X.C. Huang, Y.Y. Lin, J.P. Zhang, X.M. Chen, Ligand-directed strategy for zeolite-type metal-organic frameworks: zinc(II) imidazolates with unusual zeolitic topologies, Angew Chem. Int. Ed. Engl. 45 (2006) 1557–1559.
[12] X.-W. Liu, T.-J. Sun, J.-L. Hu, S.-D. Wang, Composites of metal–organic frameworks and carbon-based materials: preparations, functionalities and applications, J. Mater. Chem. 4 (2016) 3584–3616.
[13] Y. Du, R.Z. Chen, J.F. Yao, H.T. Wang, Facile fabrication of porous ZnO by thermal treatment of zeolitic imidazolate framework-8 and its photocatalytic activity, J. Alloy. Comp. 551 (2013) 125–130.
[14] X. Liu, L. He, J. Zheng, J. Guo, F. Bi, X. Ma, K. Zhao, Y. Liu, R. Song, Z. Tang, Solar-light-driven renewable butanol separation by core-shell Ag@ZIF-8 nanowires, Adv. Mater. 27 (2015) 3273–3277.
[15] J. Zheng, C. Cheng, W.-J. Fang, C. Chen, R.-W. Yan, H.-X. Huai, C.-C. Wang, Surfactant-free synthesis of a Fe_3O_4@ZIF-8 core–shell heterostructure for adsorption of methylene blue, CrystEngComm 16 (2014) 3960.
[16] H. Gan, Z. Wang, H. Li, Y. Wang, L. Sun, Y. Li, CdSe QDs@UIO-66 composite with enhanced photocatalytic activity towards RhB degradation under visible-light irradiation, RSC Adv. 6 (2016) 5192–5197.
[17] D. Wang, R. Huang, W. Liu, D. Sun, Z. Li, Fe-based MOFs for photocatalytic CO_2 reduction: role of coordination unsaturated sites and dual excitation pathways, ACS Catal. 4 (2014) 4254–4260.
[18] W. Wang, X. Xu, W. Zhou, Z. Shao, Recent progress in metal-organic frameworks for applications in electrocatalytic and photocatalytic water splitting, Adv. Sci. 4 (2017) 1600371.
[19] H.-P. Jing, C.-C. Wang, Y.-W. Zhang, P. Wang, R. Li, Photocatalytic degradation of methylene blue in ZIF-8, RSC Adv. 4 (2014) 54454–54462.
[20] J.G. Santaclara, M.A. Nasalevich, S. Castellanos, W.H. Evers, F.C.M. Spoor, K. Rock, L.D.A. Siebbeles, F. Kapteijn, F. Grozema, A. Houtepen, J. Gascon, J. Hunger, M.A. van der Veen, Organic linker defines the excited-state decay of photocatalytic MIL-125(Ti)-Type materials, ChemSusChem 9 (2016) 388–395.
[21] Y. Gao, S. Li, Y. Li, L. Yao, H. Zhang, Accelerated photocatalytic degradation of organic pollutant over metal-organic framework MIL-53(Fe) under visible LED light mediated by persulfate, Appl. Catal. B Environ. 202 (2017) 165–174.
[22] X. Zeng, L. Huang, C. Wang, J. Wang, J. Li, X. Luo, Sonocrystallization of ZIF-8 on electrostatic spinning TiO_2 nanofibers surface with enhanced photocatalysis property through synergistic effect, ACS Appl. Mater. Interfaces 8 (2016) 20274–20282.
[23] Q. Liu, Z.-X. Low, L. Li, A. Razmjou, K. Wang, J. Yao, H. Wang, ZIF-8/Zn_2GeO_4 nanorods with an enhanced CO_2 adsorption property in an aqueous medium for photocatalytic synthesis of liquid fuel, J. Mater. Chem. 1 (2013) 11563.
[24] R. Wang, L. Gu, J. Zhou, X. Liu, F. Teng, C. Li, Y. Shen, Y. Yuan, Quasi-polymeric metal-organic framework UiO-66/g-C_3N_4Heterojunctions for enhanced photocatalytic hydrogen evolution under visible light irradiation, Adv. Mater. Interfaces 2 (2015) 1500037.
[25] M. Wang, J. Liu, C. Guo, X. Gao, C. Gong, Y. Wang, B. Liu, X. Li, G.G. Gurzadyan, L. Sun, Metal–organic frameworks (ZIF-67) as efficient cocatalysts for photocatalytic reduction of CO_2: the role of the morphology effect, J. Mater. Chem. 6 (2018) 4768–4775.
[26] A. Schejn, A. Aboulaich, L. Balan, V. Falk, J. Lalevée, G. Medjahdi, L. Aranda, K. Mozet, R. Schneider, Cu^{2+}-doped zeolitic imidazolate frameworks (ZIF-8): efficient and stable catalysts for cycloadditions and condensation reactions, Catal. Sci. Technol. 5 (2015) 1829–1839.
[27] D. Saliba, M. Ammar, M. Rammal, M. Al-Ghoul, M. Hmadeh, Crystal growth of ZIF-8, ZIF-67, and their mixed-metal derivatives, J. Am. Chem. Soc. 140 (2018) 1812–1823 .
[28] K. Wilke, H.D. Breuer, The influence of transition metal doping on the physical and photocatalytic properties of titania, J. Photochem. Photobiol. A Chem. 121 (1999) 49–53.
[29] H. Li, X. He, Z. Kang, H. Huang, Y. Liu, J. Liu, S. Lian, C.H. Tsang, X. Yang, S.T. Lee, Water-soluble fluorescent carbon quantum dots and photocatalyst design, Angew Chem. Int. Ed. Engl. 49 (2010) 4430–4434.
[30] Y. Huang, Y. Liang, Y. Rao, D. Zhu, J.J. Cao, Z. Shen, W. Ho, S.C. Lee, Environment-friendly carbon quantum dots/$ZnFe_2O_4$ photocatalysts: characterization, biocompatibility, and mechanisms for NO removal, Environ. Sci. Technol. 51 (2017) 2924–2933.
[31] H. Ming, Z. Ma, Y. Liu, K. Pan, H. Yu, F. Wang, Z. Kang, Large scale electrochemical synthesis of high quality carbon nanodots and their photocatalytic property, Dalton Trans. 41 (2012) 9526–9531.
[32] H. Yu, Y. Zhao, C. Zhou, L. Shang, Y. Peng, Y. Cao, L.-Z. Wu, C.-H. Tung, T. Zhang, Carbon quantum dots/TiO_2 composites for efficient photocatalytic hydrogen evolution, J. Mater. Chem. 2 (2014) 3344.
[33] H. Zhang, H. Huang, H. Ming, H. Li, L. Zhang, Y. Liu, Z. Kang, Carbon quantum dots/Ag_3PO_4 complex photocatalysts with enhanced photocatalytic activity and stability under visible light, J. Mater. Chem. 22 (2012) 10501.
[34] F. Duo, Y. Wang, C. Fan, X. Zhang, Y. Wang, Enhanced visible light photocatalytic activity and stability of CQDs/BiOBr composites: the upconversion effect of CQDs, J. Alloy. Comp. 685 (2016) 34–41.
[35] J. Liu, R. Li, Y. Wang, Y. Wang, X. Zhang, C. Fan, The active roles of ZIF-8 on the enhanced visible photocatalytic activity of Ag/AgCl: generation of superoxide radical and adsorption, J. Alloy. Comp. 693 (2017) 543–549.
[36] W. Sun, X. Zhai, L. Zhao, Synthesis of ZIF-8 and ZIF-67 nanocrystals with well-controllable size distribution through reverse microemulsions, Chem. Eng. J. 289 (2016) 59–64.
[37] K. Zhou, B. Mousavi, Z. Luo, S. Phatanasri, S. Chaemchuen, F. Verpoort, Characterization and properties of Zn/Co zeolitic imidazolate frameworks vs. ZIF-8 and ZIF-67, J. Mater. Chem. 5 (2017) 952–957.
[38] H. Zhang, H. Ming, S. Lian, H. Huang, H. Li, L. Zhang, Y. Liu, Z. Kang, S.T. Lee, Fe_2O_3/carbon quantum dots complex photocatalysts and their enhanced photocatalytic activity under visible light, Dalton Trans. 40 (2011) 10822–10825.
[39] Y. Li, A. Pang, C. Wang, M. Wei, Metal–organic frameworks: promising materials for improving the open circuit voltage of dye-sensitized solar cells, J. Mater. Chem. 21 (2011) 17259.
[40] P.Z. Li, K. Aranishi, Q. Xu, ZIF-8 immobilized nickel nanoparticles: highly effective catalysts for hydrogen generation from hydrolysis of ammonia borane, Chem Commun (Camb) 48 (2012) 3173–3175.
[41] M. Jian, B. Liu, G. Zhang, R. Liu, X. Zhang, Adsorptive removal of arsenic from aqueous solution by zeolitic imidazolate framework-8 (ZIF-8) nanoparticles, Colloid. Surf. Physicochem. Eng. Asp. 465 (2015) 67–76.
[42] X. Wu, C. Yang, J. Ge, Z. Liu, Polydopamine tethered enzyme/metal-organic framework composites with high stability and reusability, Nanoscale 7 (2015) 18883–18886.
[43] K. Jayaramulu, K.K. Datta, C. Rosler, M. Petr, M. Otyepka, R. Zboril, R.A. Fischer, Biomimetic superhydrophobic/superoleophilic highly fluorinated graphene

oxide and ZIF-8 composites for oil-water separation, Angew Chem. Int. Ed. Engl. 55 (2016) 1178–1182.
[44] H. Wang, X. Yuan, Y. Wu, G. Zeng, X. Chen, L. Leng, H. Li, Synthesis and applications of novel graphitic carbon nitride/metal-organic frameworks mesoporous photocatalyst for dyes removal, Appl. Catal. B Environ. 174–175 (2015) 445–454.
[45] B.P. Biswal, D.B. Shinde, V.K. Pillai, R. Banerjee, Stabilization of graphene quantum dots (GQDs) by encapsulation inside zeolitic imidazolate framework nanocrystals for photoluminescence tuning, Nanoscale 5 (2013) 10556–10561.
[46] J. Ke, X. Li, Q. Zhao, B. Liu, S. Liu, S. Wang, Upconversion carbon quantum dots as visible light responsive component for efficient enhancement of photocatalytic performance, J. Colloid Interface Sci. 496 (2017) 425–433.
[47] F. Wang, Z.S. Liu, H. Yang, Y.X. Tan, J. Zhang, Hybrid zeolitic imidazolate frameworks with catalytically active TO_4 building blocks, Angew Chem. Int. Ed. Engl. 50 (2011) 450–453.
[48] M.B. Chambers, X. Wang, L. Ellezam, O. Ersen, M. Fontecave, C. Sanchez, L. Rozes, C. Mellot-Draznieks, Maximizing the photocatalytic activity of metal-organic frameworks with aminated-functionalized linkers: substoichiometric effects in MIL-125-NH2, J. Am. Chem. Soc. 139 (2017) 8222–8228.
[49] J. Liu, R. Li, Y. Hu, T. Li, Z. Jia, Y. Wang, Y. Wang, X. Zhang, C. Fan, Harnessing Ag nanofilm as an electrons transfer mediator for enhanced visible light photocatalytic performance of Ag@AgCl/Ag nanofilm/ZIF-8 photocatalyst, Appl. Catal. B Environ. 202 (2017) 64–71.
[50] Z. Wang, Y. Huang, W. Ho, J. Cao, Z. Shen, S.C. Lee, Fabrication of $Bi_2O_2CO_3$/g-C_3N_4 heterojunctions for efficiently photocatalytic NO in air removal: in-situ self-sacrificial synthesis, characterizations and mechanistic study, Appl. Catal. B Environ. 199 (2016) 123–133.
[51] M. Chen, Y. Huang, J. Yao, J.-j. Cao, Y. Liu, Visible-light-driven N-$(BiO)_2CO_3$/Graphene oxide composites with improved photocatalytic activity and selectivity for NOx removal, Appl. Surf. Sci. 430 (2018) 137–144.
[52] Y. Huang, Y. Gao, Q. Zhang, Y. Zhang, J.J. Cao, W. Ho, S.C. Lee, Biocompatible FeOOH-Carbon quantum dots nanocomposites for gaseous NOx removal under visible light: improved charge separation and High selectivity, J. Hazard Mater. 354 (2018) 54–62.
[53] Y.-Q. Zhang, D.-K. Ma, Y.-G. Zhang, W. Chen, S.-M. Huang, N-doped carbon quantum dots for TiO_2-based photocatalysts and dye-sensitized solar cells, Nanomater. Energy 2 (2013) 545–552.
[54] Y. Zhang, N. Zhang, Z.-R. Tang, Y.-J. Xu, Graphene transforms wide band gap ZnS to a visible light photocatalyst. The new role of graphene as a macromolecular photosensitizer, ACS Nano 6 (2012) 9777–9789.
[55] Q. Zhang, Y. Huang, S. Peng, Y. Zhang, Z. Shen, J.-j. Cao, W. Ho, S.C. Lee, D.Y.H. Pui, Perovskite $LaFeO_3$-$SrTiO_3$ composite for synergistically enhanced NO removal under visible light excitation, Appl. Catal. B Environ. 204 (2017) 346–357.
[56] C. Gao, J. Wang, H. Xu, Y. Xiong, Coordination chemistry in the design of heterogeneous photocatalysts, Chem. Soc. Rev. 46 (2017) 2799–2823.
[57] M.A. Nasalevich, M. van der Veen, F. Kapteijn, J. Gascon, Metal–organic frameworks as heterogeneous photocatalysts: advantages and challenges, CrystEngComm 16 (2014) 4919–4926.
[58] M. Alvaro, E. Carbonell, B. Ferrer, F.X. Llabres i Xamena, H. Garcia, Semiconductor behavior of a metal-organic framework (MOF), Chemistry 13 (2007) 5106–5112.
[59] C.-C. Wang, J.-R. Li, X.-L. Lv, Y.-Q. Zhang, G. Guo, Photocatalytic organic pollutants degradation in metal–organic frameworks, Energy Environ. Sci. 7 (2014) 2831–2867.
[60] K.T. Butler, C.H. Hendon, A. Walsh, Electronic chemical potentials of porous metal-organic frameworks, J. Am. Chem. Soc. 136 (2014) 2703–2706.
[61] M. Li, Z. Zheng, Y. Zheng, C. Cui, C. Li, Z. Li, Controlled growth of metal-organic framework on upconversion nanocrystals for NIR-enhanced photocatalysis, ACS Appl. Mater. Interfaces 9 (2017) 2899–2905.
[62] S. Panneri, M. Thomas, P. Ganguly, B.N. Nair, A.P. Mohamed, K.G.K. Warrier, U.S. Hareesh, C_3N_4 anchored ZIF 8 composites: photo-regenerable, high capacity sorbents as adsorptive photocatalysts for the effective removal of tetracycline from water, Catal. Sci. Technol. 7 (2017) 2118–2128.
[63] Z. Wang, Y. Huang, L. Chen, M. Chen, J. Cao, W. Ho, S.C. Lee, In situ g-C_3N_4 self-sacrificial synthesis of a g-C_3N_4/$LaCO_3OH$ heterostructure with strong interfacial charge transfer and separation for photocatalytic NO removal, J. Mater. Chem. 6 (2018) 972–981.